

A Stable Measure of Chaos in Dynamical Systems Using Persistent Homology

Bala Krishnamoorthy^{*}¹ and Elizabeth P. Thompson[†]¹

¹Department of Mathematics and Statistics, Washington State University

Abstract

Many real-world dynamics exhibit chaos, a phenomenon in which neighboring trajectories in the state space of a dynamical system diverge exponentially over time. A common measure used for measuring the degree of this divergence is the Lyapunov exponent, which relies on pairwise Euclidean distances between the trajectories at each time. The main limitation of the Lyapunov exponent is its sensitivity to small perturbations in input data. Since many real-world dynamics are likely to contain some degree of inherent noise, we are motivated to construct a chaos measure that is robust to small trajectory perturbations. Persistent homology has been used for proving theoretical stability guarantees under such added noise in the data. As such, we introduce a novel, persistent homology based measure of chaos termed the persistence exponent and prove its theoretical stability. We also prove the existence of an upper bound on our measure, and show its greater experimental stability on the Lorenz and Rossler systems describing fluid convection and taffy pulling. We present an algorithm for computing the persistence exponent given a single time series with N points from a dynamical system that runs in $O(N^2 \log N)$ time. We finally show the greater experimental stability of the persistence exponent on time series data depicting a Belousov Zhabotinsky chemical reaction, which transitions from periodicity to chaos and back as the system evolves in time.

1 Dynamical Systems and Chaos

Many real-world systems can be characterized by differential equations describing the dynamics of a collection of parameters over time. As such, they are commonly referred to as dynamical systems, which model a variety of phenomenon including but not limited to fluid dynamics, population growth, and chemical reactions. Dynamical systems are typically studied via their trajectories in state space, which, given an initial condition of the system, are obtained by integrating its differentials to yield a collection of time series and plotting these series together as multidimensional points in Euclidean space. Another common approach is to apply a sliding windows embedding to a single time series to produce a state space trajectory for the system [12, 8]. A system feature of particular interest are control parameters that drastically change the system's behavior. Commonly studied behaviors are periodicity and chaoticity, and the study of which control parameters influence a system to behave in either of these fashions, and the extent of chaos when present. Intuitively, a system is periodic if its state space exhibits “loop-like” structure, in which as one traverses a point cloud trajectory, locations are revisited at a given frequency. On the other hand, a system is considered chaotic if as one traverses two neighboring trajectories, they become exponentially farther apart over time, a phenomenon referred to as the exponential divergence of nearby trajectories [5]. Several methods have been used to study periodicity and chaos, such as quantifying ([5, 14]) or detecting ([4, 11, 16, 18]) these behaviors, as well as approximating the dimension of the geometric space occupied by a state-space trajectory

^{*}kbala@wsu.edu, <https://orcid.org/0000-0002-2727-6547>

[†]Corresponding author: elizabeth.thompson1@wsu.edu, <https://orcid.org/0009-0000-0268-9188>

([7, 3]). We provide an example in Figure 1 of a well known dynamical system, the Lorenz attractor (see subsection 8.1 for details). This system models fluid convection and is defined by three differentials, which when integrated produce three time series in state space (\mathbb{R}^3). We show a chaotic system on the top and a periodic system on the bottom.

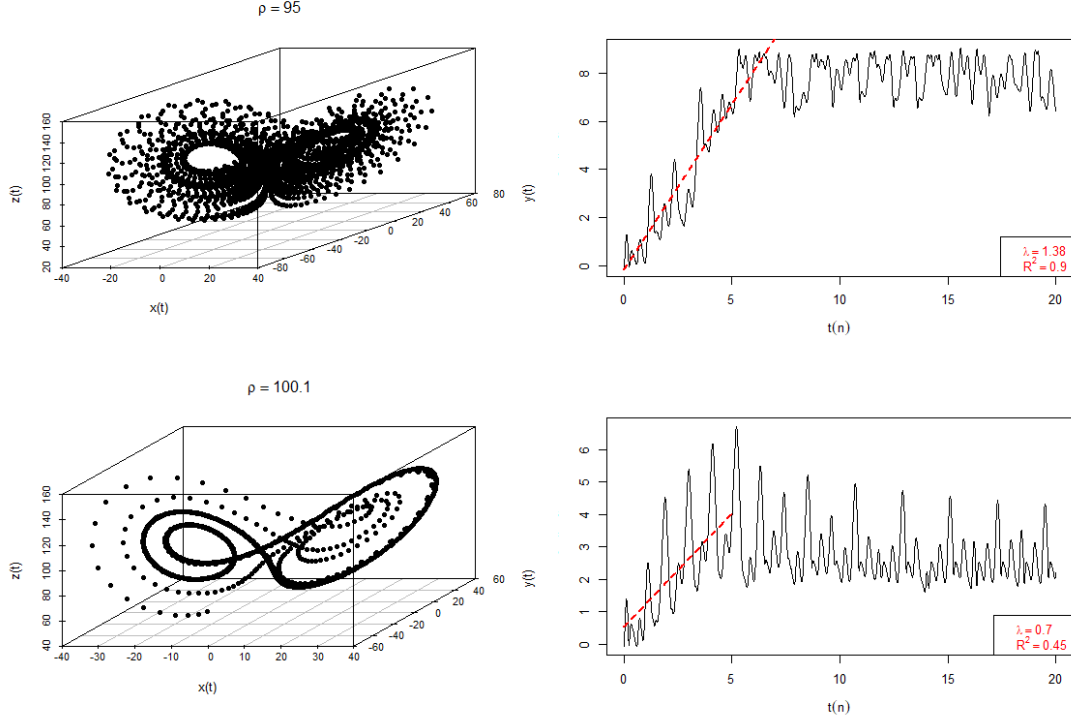


Figure 1: A chaotic (top left) and periodic (bottom left) Lorenz system, as well as their respective Lyapunov exponent measurements (top right and bottom right). ρ is the control parameter varied to detect changes in system behavior (see subsection 8.1 for details).

2 Limitations of Measuring Chaos

A common method for quantifying the chaos in a dynamical system given a pair of its neighboring trajectories (i.e., those whose initial conditions are close) is via the Lyapunov exponent. This exponent measures the rate of exponential divergence of two neighboring trajectories over time in state space. A more positive Lyapunov exponent indicates more chaos, whereas less positive, zero, or negative values indicate periodicity [5, 14]. In the right column of Figure 1, we show an example of the Lyapunov exponent for a chaotic and a periodic Lorenz system. We can see that when the system is chaotic, the estimated Lyapunov exponent is larger (1.38 vs 0.7).

One of the main practical limitations of the Lyapunov exponent is its lack of robustness to added noise in system trajectories. Since this measure relies on Euclidean distance alone for its computation, we suspect that it is more sensitive to small perturbations in the trajectories. We show an example in Figure 2 of its instability when measuring chaos in the Lorenz system with added noise. We plot the average Lyapunov exponent over 20 pairs of initial conditions and Gaussian noise levels σ , where for each trajectory point $\mathbf{x} \in \mathbb{R}^3$, we define its perturbation in the d th direction as $\mathbf{x}_\sigma^d = \mathbf{x}_d + \sigma \cdot \gamma_d$, where γ_d is the standard deviation of \mathbf{x}_d , the d th dimension of \mathbf{x} . Notice that when we add just 2.5% noise (i.e., $\sigma = 0.025$) to

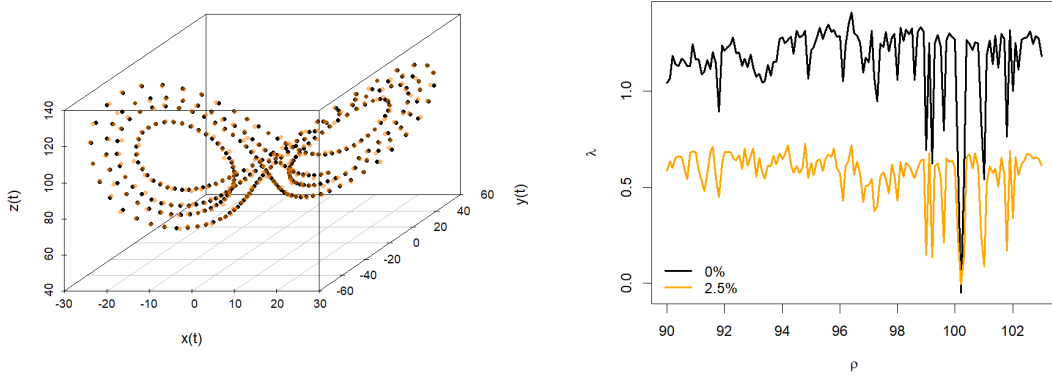


Figure 2: A chaotic Lorenz trajectory for the last 3 seconds with 2.5% added Gaussian noise when $\rho = 95$ (left), and the average Lyapunov exponents over 20 pairs of neighboring trajectories (right). There is a marked decrease in the Lyapunov exponent even for the small amount of noise added.

a pair of neighboring trajectories, the average Lyapunov exponent drops substantially. Since dynamical systems model real-world phenomena, we expect there to be some inherent system noise. On the other hand, persistent homology studies holes that appear as one thickens the points in a metric space over time, and has proven theoretical stability to small data perturbations [1, 12]. As such, we construct a persistence-based measure of chaos that is stable to such added noise, which we term the *persistence exponent*.

3 Contributions and Organization

We define a novel measure of chaos in dynamical systems based on persistent homology termed the *persistence exponent* (Theorem 4.15). Unlike the commonly used Lyapunov exponent (Theorem 4.5), the persistence exponent is stable to small perturbations in input data. We prove the theoretical stability of the persistence exponent (Theorem 6.1) as well as show its greater experimental stability on the Lorenz (Figure 3) and the Rossler (Figure 4) systems. We also derive theoretical upper and lower bounds on the persistence exponent (Theorem 6.4), which allow us to deduce the maximum possible exponential divergence of two neighboring trajectories between any range of filtration parameters. We present an algorithm to compute the persistence exponent from a single time series embedding (algorithm 2) and deduce its computational complexity (Theorem 7.1). We finally use our algorithm to show greater experimental stability of the persistence exponent when compared to the Lyapunov exponent on real time series data describing the change in concentration of a catalyst in an autocatalytic chemical reaction over time (Figure 6).

We introduce definitions related to dynamical systems (subsection 4.1), persistent homology (subsection 4.2), and our persistence exponent (subsection 4.3). We then outline previous work done in both detecting and quantifying periodicity and chaos in dynamical systems, followed by a brief review of the theoretical stability of persistent homology (section 5). Following this discussion, we formally introduce our persistence exponent and the intuition behind its construction, as well as our proof of its stability and its bounds (section 6). In section 7, we present our algorithm for computing the persistence exponent on real time series data and discuss its computational complexity. We then present experimental results that highlight the greater stability of our persistence exponent on various dynamical systems with known behavior (subsection 8.1 and subsection 8.2), as well as on real time series data (subsection 8.3). We end with discussion and future work in section 9.

4 Definitions

4.1 Dynamical Systems and Chaos

This section contains an overview of necessary terminology regarding dynamical systems and chaos. More information can be found in, e.g., the book by Hilborn [5].

Definition 4.1 (Dynamical System). *A **dynamical system** X is a system whose dynamics can be modeled by a collection of p differential equations $\left\{ \frac{d\dot{X}_1(\mathbf{A},t)}{dt}, \dots, \frac{d\dot{X}_p(\mathbf{A},t)}{dt} \right\}$, each as a function of time $t \in \mathcal{T}$ and m control parameters $\mathbf{A} = \{A_1, \dots, A_m\}$.*

Definition 4.2 (State Space). *The **state space** of a dynamical system X is given by $(\dot{X}_1(\mathbf{A},t), \dots, \dot{X}_p(\mathbf{A},t)) \in \mathbb{R}^p$ for $t \in \mathcal{T}$.*

Definition 4.3 (Trajectory). *The **trajectory** of a dynamical system X in its state space evaluated at times $\mathcal{T} = \{t_0, \dots, t_{T-1}\}$ for $T \in \mathbb{N}$ is given by $\mathbf{x}_A(\mathcal{T}) = \{\mathbf{x}_A(t_0), \dots, \mathbf{x}_A(t_{T-1})\}$ where $\mathbf{x}_A(t_n) = (\dot{X}_1(\mathbf{A}, t_n), \dots, \dot{X}_p(\mathbf{A}, t_n)) \in \mathbb{R}^p$.*

Definition 4.4 (Neighboring trajectories). *Given an initial condition $\mathbf{x}_A(t_0)$ of a dynamical system X , we define its corresponding trajectory as $\mathbf{x}_A(\mathcal{T})$. Another trajectory $\mathbf{y}_A(\mathcal{T})$ is a **neighboring trajectory** of $\mathbf{x}_A(\mathcal{T})$ if $\|\mathbf{x}_A(t_0) - \mathbf{y}_A(t_0)\|$ is sufficiently small.*

Definition 4.5 (Lyapunov Exponent). *Given a pair of neighboring trajectories $\mathbf{x}_A(\mathcal{T})$ and $\mathbf{y}_A(\mathcal{T})$ in the state space of a dynamical system X , the **Lyapunov exponent** of X is given by $\lambda = \lim_{n \rightarrow \infty} \log \left(\frac{d_n}{d_0} \right)$, where $d_n = \|\mathbf{x}_A(t_n) - \mathbf{y}_A(t_n)\|$ and $d_0 = \|\mathbf{x}_A(t_0) - \mathbf{y}_A(t_0)\|$.*

4.2 Persistent Homology and Distance Metrics

This section provides necessary definitions of persistent homology and distance metrics for topological summaries. More information can be found in relevant publications [15, 17].

Definition 4.6 (Vietoris-Rips Complex). *Given a point cloud $X \in \mathbb{R}^n$ and a positive radius $\epsilon > 0$, the **Vietoris-Rips complex** of X at ϵ is given by $\mathcal{R}_\epsilon(X) = \{\sigma \subset X : \|\mathbf{x}_i - \mathbf{x}_j\| \leq 2\epsilon, \forall \mathbf{x}_i, \mathbf{x}_j \in \sigma\}$.*

Definition 4.7 (Vietoris-Rips Filtration). *Given a point cloud $X \in \mathbb{R}^n$ and a collection of positive radii $\{\epsilon_1 = 0, \dots, \epsilon_R\}$, the **Vietoris-Rips filtration** of X is given by the nested sequence of subcomplexes $\mathcal{R}_{\epsilon_1}(X) = X \subset \mathcal{R}_{\epsilon_2}(X) \subset \dots \subset \mathcal{R}_{\epsilon_R}(X)$.*

Definition 4.8 (Persistence Barcode). *The **persistence barcode** of a point cloud $X \in \mathbb{R}^n$ is given by $\text{Bcd}(\mathcal{R}(X)) = \{[b_p^i, d_p^i] : p = 0, 1, \dots, i = 1, \dots, m_p\}$, where $d_p^i - b_p^i$ is the lifetime of the i -th p -dimensional class of holes in the Vietoris-Rips filtration on X .*

Definition 4.9 (Betti Number). *Given the persistence barcode of a point cloud $X \in \mathbb{R}^n$, the p -th **Betti number** of X at filtration radius $\epsilon > 0$ is given by $\beta_p^\epsilon(X) = \sum_{i=1}^{m_p} \delta_\epsilon([b_p^i, d_p^i])$, where $\delta_\epsilon([b_p^i, d_p^i]) = 1$ if $b_p^i \leq \epsilon < d_p^i$ and is zero otherwise.*

Definition 4.10 (Correspondence). *A **correspondence** f between two metric spaces (X, d_X) and (Y, d_Y) is a relation on $X \times Y$ such that for all $\mathbf{x}, \mathbf{x}' \in X$, there exists some $\mathbf{y}, \mathbf{y}' \in Y$ such that $f(\mathbf{x}') = \mathbf{x}'$ and $f(\mathbf{y}) = \mathbf{y}'$.*

Definition 4.11 (Distortion). *Given two metric spaces (X, d_X) and (Y, d_Y) , the **distortion** of a correspondence f between them is given by $\text{dis}(f) = \sup_{\mathbf{x}, \mathbf{x}'} \left\{ \left| \|\mathbf{x} - \mathbf{x}'\| - \|f(\mathbf{x}) - f(\mathbf{x}')\| \right| \right\}$ for $\mathbf{x}, \mathbf{x}' \in X$.*

Definition 4.12 (Gromov-Hausdorff Distance). *The **Gromov-Hausdorff distance** between two metric spaces (X, d_X) and (Y, d_Y) is given by $d_{\text{GH}}(X, Y) = \frac{1}{2} \inf\{\text{dis}(f)\}$ among all possible correspondences f on $X \times Y$.*

Definition 4.13 (Interleaving Distance). *The **interleaving distance** between two non-increasing piecewise constant functions $g, h : [0, \infty) \rightarrow [0, \infty)$ is given by $d_I(g, h) = \inf\{\alpha > 0 : g(v) \geq h(v + \alpha), h(v) \geq g(v + \alpha)\}$ for all $v \in [0, \infty)$.*

4.3 The Persistence Exponent

We now state a special case of the interleaving distance that measures the change between two p -dimensional Betti curves. We then provide the definition of our novel persistence-based measure of chaos in dynamical systems.

Definition 4.14 (Interleaving Distance Between Betti Curves). *Given a pair of neighboring trajectories $Z = \mathbf{x}_A(\mathcal{T}) \cup \mathbf{y}_A(\mathcal{T})$, their perturbation $Z' = \mathbf{x}'_A(\mathcal{T}) \cup \mathbf{y}'_A(\mathcal{T})$, and a partition of filtration radii $0 = \epsilon_1 < \dots < \epsilon_R$, we define the r -th p -dimensional Betti curve of Z and Z' as the non-increasing piecewise constant functions $\beta_p^{\epsilon_r}(Z), \beta_p^{\epsilon_r}(Z') : [0, \epsilon_R] \rightarrow [0, 2T]$. The **interleaving distance** between the Betti curves is given by $d_I(\beta_p^{\epsilon_r}(Z), \beta_p^{\epsilon_r}(Z')) = \inf\{\alpha > 0 : \beta_p^{\epsilon_r}(Z) \geq \beta_p^{\epsilon_r+\alpha}(Z'), \beta_p^{\epsilon_r}(Z') \geq \beta_p^{\epsilon_r+\alpha}(Z)\}$.*

Definition 4.15 (Persistence Exponent). *The **persistence exponent** of a dynamical system X is given by $\beta_{\text{exp}}(X) = \lim_{r \rightarrow \infty} -\log \left(\frac{\beta_0^{\epsilon_r}(Z)}{\beta_0^{\epsilon_1}(Z)} \right)$, where $\beta_0^{\epsilon_r}(Z)$ is the r -th Betti curve corresponding to the neighboring trajectories $Z = \mathbf{x}_A(\mathcal{T}) \cup \mathbf{y}_A(\mathcal{T})$ and $Z' = \mathbf{x}'_A(\mathcal{T}) \cup \mathbf{y}'_A(\mathcal{T})$ in the state space of X . Unless otherwise stated, we let $\epsilon_1 = 0$ so that $\beta_0^{\epsilon_1}(Z) = 2T$.*

5 Related Work

One common method used to detect chaos in a dynamical system is through a bifurcation diagram [5]. This is typically a plot of the local extrema of one time series defining a dynamical system against varying values of a control parameter. These diagrams are used to determine the control parameters for which a system is chaotic or periodic. A widely used measure for quantifying chaos in a system X given a pair of its neighboring trajectories (Theorem 4.4) in state space is the Lyapunov exponent (Theorem 4.5), which we denote by λ . The Lyapunov exponent measures the rate of exponential divergence (in Euclidean distance) of two neighboring trajectories over time in state space [5, 14]. Positive values of λ typically indicate chaos, whereas zero or negative values of λ indicate periodicity. Persistent homology has also been used to detect system bifurcations using topological summaries called CROCKER plots [11]. CROCKER plots of dynamical systems are heatmaps of p -dimensional Betti numbers for increasing filtration parameters against increasing values of a given control parameter, and Mittal and Gupta [11] experimentally discovered similarities between the behavior of the Lyapunov exponent and that of the Betti vector norm of the columns in the 1-CROCKER plot of a Lorenz system against increasing values of a control parameter. More recently, persistent homology has been used to predict chaotic behavior in the Rossler system [6], where the authors used Betti curves from Vietoris-Rips filtration to produce stable classifications of dynamics for varying control parameters. It is known that trajectories (Theorem 4.3) of chaotic systems must exist in at least three dimensions [5]. These systems can be highly complex and persistent homology has become a popular method for measuring the dimension of the geometric space embedding chaotic trajectories [7]. The main intuition is that more chaotic systems will produce higher growth rates and hence take up larger geometric dimensions in state space.

Persistent homology has been proven to be stable to small perturbations in input data [1, 10]. Specifically, given a pair of metric spaces (X, d_X) and (Y, d_Y) and their corresponding persistence barcodes $\text{Bcd}(\mathcal{R}(X))$ and $\text{Bcd}(\mathcal{R}(Y))$, the following relation is guaranteed to hold:

$$d_I \left(\text{Bcd}(\mathcal{R}(X)), \text{Bcd}(\mathcal{R}(Y)) \right) \leq 2 d_{\text{GH}}(X, Y).$$

That is, small changes in X as measured by the Gromov-Hausdorff distance lead to only small changes in $\text{Bcd}(\mathcal{R}(X))$ as measured by the interleaving distance. This stability is the key motivation for our construction of the persistence exponent (Theorem 4.15) as a stable alternative to the Lyapunov exponent to measure chaos in dynamical systems.

6 The Persistence Exponent and Stability

We now introduce a novel, persistence-based measure of chaos termed the persistence exponent, which we denote as β_{exp} . Given a pair of neighboring trajectories $\mathbf{x}_A(\mathcal{T})$ and $\mathbf{y}_A(\mathcal{T})$ in state space of a dynamical system X , we analyze the evolution of the connected components in the Vietoris-Rips filtration $\mathcal{R}(Z)$ of their union $Z = \mathbf{x}_A(\mathcal{T}) \cup \mathbf{y}_A(\mathcal{T})$ over time. The main intuition is that we expect periodic trajectories to contain points that merge much more quickly at first, leaving less connected components to merge later on and hence producing a lower rate of merging long term. On the other hand, chaotic trajectories contain points that are likely to take exponentially longer to merge as the filtration radius increases, which produce higher rates of merging in the long term. We capture the rate of merging of connected components of $\mathcal{R}(Z)$ via the rate of growth in the negative logarithm of the number of connected components over time, where time indicates the filtration radius. Moreover, we hypothesize that chaotic systems with sufficiently large enough degrees of exponential divergence satisfy the relationship $\beta_0(\epsilon_r) = \beta_0(\epsilon_1)e^{-\beta_{\text{exp}} \cdot \epsilon_r}$, where the number of connected components decreases exponentially as a function of the filtration radius. Hence, the rate of exponential divergence is given by

$$\beta_{\text{exp}}(X) = \lim_{r \rightarrow \infty} -\log \left(\frac{\beta_0^{\epsilon_r}(Z)}{\beta_0^{\epsilon_1}(Z)} \right).$$

Using stability properties of persistent homology, we prove that small changes in a pair of neighboring trajectories of a dynamical system guarantee small changes in the 0-dimensional Betti curve of their union. Hence we prove stability of the persistence exponent to small perturbations in the neighboring trajectories of dynamical system's state space.

Theorem 6.1 (Stability of the Persistence Exponent). *Let $(Z = \mathbf{x}_A(\mathcal{T}) \cup \mathbf{y}_A(\mathcal{T}), \|\cdot\|)$ and $(Z' = \mathbf{x}'_A(\mathcal{T}) \cup \mathbf{y}'_A(\mathcal{T}), \|\cdot\|)$ be two pairs of neighboring trajectories in the state space of a dynamical system X where $\mathcal{T} = \{t_0, \dots, t_{T-1}\}$. Given a partition $0 = \epsilon_1 < \dots < \epsilon_r < \dots < \epsilon_R$ of Vietoris-Rips filtration radii, the following relation holds:*

$$d_I(\beta_0^{\epsilon_r}(Z), \beta_0^{\epsilon_r}(Z')) \leq 2d_{\text{GH}}(Z, Z'),$$

where $\beta_0^{\epsilon_r}(Z), \beta_0^{\epsilon_r}(Z') : [0, \epsilon_R] \rightarrow [0, 2T]$.

Proof. Suppose $d_{\text{GH}}(Z, Z') = \gamma$. Then for all correspondences f on $Z \times Z'$, we have that $\inf\{\text{dis}(f)\} = 2\gamma$. Then there must exist some correspondence f^* such that

$$\text{dis}(f^*) = \sup_{\mathbf{z}_i, \mathbf{z}_j \in Z} \left\{ \left| \|\mathbf{z}_i - \mathbf{z}_j\| - \|f^*(\mathbf{z}_i) - f^*(\mathbf{z}_j)\| \right| \right\} = 2\gamma.$$

Hence for all $\mathbf{z}_i, \mathbf{z}_j \in Z$, $\left| \|\mathbf{z}_i - \mathbf{z}_j\| - \|f^*(\mathbf{z}_i) - f^*(\mathbf{z}_j)\| \right| \leq 2\gamma$, which implies that

$$\|\mathbf{z}_i - \mathbf{z}_j\| \leq \|f^*(\mathbf{z}_i) - f^*(\mathbf{z}_j)\| + 2\gamma \quad (1)$$

$$\|f^*(\mathbf{z}_i) - f^*(\mathbf{z}_j)\| \leq \|\mathbf{z}_i - \mathbf{z}_j\| + 2\gamma. \quad (2)$$

Claim 6.2. $\beta_0^{\epsilon_r}(Z) \geq \beta_0^{\epsilon_r+2\gamma}(Z')$.

Proof. Let (\mathbf{a}, \mathbf{b}) be an edge in $\mathcal{R}_{\epsilon_r}(Z)$. Then $\|\mathbf{a} - \mathbf{b}\| \leq \epsilon_r$ by definition. Hence by (Equation 2), $\|f^*(\mathbf{a}) - f^*(\mathbf{b})\| \leq \|\mathbf{a} - \mathbf{b}\| + 2\gamma \leq \epsilon_r + 2\gamma$. Hence $(f^*(\mathbf{a}), f^*(\mathbf{b}))$ is an edge in $\mathcal{R}_{\epsilon_r+2\gamma}(Z')$ and $\mathcal{R}_{\epsilon_r}(Z) \subseteq \mathcal{R}_{\epsilon_r+2\gamma}(Z')$. That is, the Vietoris-Rips complex of Z' at $\epsilon_r + 2\gamma$ is more connected than the Vietoris-Rips complex of Z at ϵ_r , and hence our claim holds. \square

Claim 6.3. $\beta_0^{\epsilon_r}(Z') \geq \beta_0^{\epsilon_r+2\gamma}(Z)$.

Proof. Let $(\mathbf{a}', \mathbf{b}')$ be an edge in $\mathcal{R}_{\epsilon_r}(Z')$. Then $\|\mathbf{a}' - \mathbf{b}'\| \leq \epsilon_r$ by definition. Hence there exists some $\mathbf{a}, \mathbf{b} \in Z$ such that $f^*(\mathbf{a}) = \mathbf{a}'$ and $f^*(\mathbf{b}) = \mathbf{b}'$. Hence by (Equation 1), $\|\mathbf{a} - \mathbf{b}\| \leq \|\mathbf{a}' - \mathbf{b}'\| + 2\gamma \leq \epsilon_r + 2\gamma$. Therefore, (\mathbf{a}, \mathbf{b}) is an edge in $\mathcal{R}_{\epsilon_r+2\gamma}(Z)$. Then $\mathcal{R}_{\epsilon_r}(Z') \subseteq \mathcal{R}_{\epsilon_r+2\gamma}(Z)$ and hence the Vietoris-Rips complex of Z at $\epsilon_r + 2\gamma$ is more connected than that of Z' at ϵ_r and therefore our claim is satisfied. \square

Theorem 6.2 and Theorem 6.3 together imply that 2γ is one possible candidate for the interleaving distance between the 0-dimensional Betti curves. Since this interleaving distance is the infimum of all possible solutions, we get that $d_I(\beta_0^{\epsilon_r}(Z), \beta_0^{\epsilon_r}(Z')) \leq 2\gamma = 2d_{GH}(Z, Z')$. \square

Proposition 6.4 (Bounds on the Persistence Exponent). *Let $\epsilon_{r_{\min}} < \epsilon_{r_{\max}}$ and assume that ϵ_1 need not be zero. Let β_{\exp} be the persistence exponent of a dynamical system X on a pair of neighboring trajectories $Z = \mathbf{x}_A(\mathcal{T}) \cup \mathbf{y}_A(\mathcal{T})$ for $\mathcal{T} = \{t_0, \dots, t_{T-1}\}$. If β_{\exp} was obtained via linear regression on $\Delta\epsilon = \epsilon_{r_{\max}} - \epsilon_{r_{\min}}$, then $0 \leq \beta_{\exp}(X) \leq \frac{-\log(\frac{1}{2T})}{\Delta\epsilon}$.*

Proof. Notice that $1 \leq \beta_0^{\epsilon_r}(Z) \leq \beta_0^{\epsilon_1}(Z) \leq 2T$. Then

$$\begin{aligned} \frac{1}{2T} &\leq \frac{\beta_0^{\epsilon_r}(Z)}{2T} \leq \frac{\beta_0^{\epsilon_1}(Z)}{2T} \leq 1 \\ &\implies \log\left(\frac{1}{2T}\right) \leq \log\left(\frac{\beta_0^{\epsilon_r}(Z)}{2T}\right) \leq \log\left(\frac{\beta_0^{\epsilon_1}(Z)}{2T}\right) \leq 0 \\ &\implies -\log\left(\frac{1}{2T}\right) \geq -\log\left(\frac{\beta_0^{\epsilon_r}(Z)}{2T}\right) \geq -\log\left(\frac{\beta_0^{\epsilon_1}(Z)}{2T}\right) \geq 0. \end{aligned}$$

Hence if we approximate β_{\exp} on $[\epsilon_{r_{\min}}, \epsilon_{r_{\max}}]$ (i.e., for all $r \in r_{\min}, \dots, r_{\max}$), then we obtain our result. \square

7 An Algorithm for Computing the Persistence Exponent

With real data, we typically have access to only a single time series. In this case, chaos is often quantified locally within a single time series embedding. The Kantz algorithm [8] estimates the maximum Lyapunov exponent of a single trajectory in the state space embedding of a univariate time series. We present our pseudocode for computing the Kantz Lyapunov exponent in algorithm 1. Given the i -th observation $\mathbf{x}_i \in \mathbb{R}^d$ in a time series embedding with N points, the average Euclidean distance between it and its neighbors is given by

$$L_i = \frac{1}{|N_\delta(\mathbf{x}_i)|} \sum_{j=1}^{|N_\delta(\mathbf{x}_i)|} \|\mathbf{x}_i - \mathbf{x}_j\|, \quad (3)$$

where \mathbf{x}_j is the j -th neighbor of \mathbf{x}_i in its δ neighborhood $N_\delta(\mathbf{x}_i) = \{\mathbf{x}_j : \|\mathbf{x}_i - \mathbf{x}_j\| < \delta\}$. Moving forward t steps in time, the δ -neighborhood of the $(i+t)$ -th point is given by $N_\delta(\mathbf{x}_{i+t}) = \{\mathbf{x}_{j+t} : \mathbf{x}_j \in N_\delta(\mathbf{x}_i)\}$ for $t = 1, \dots, t_{\max}$. Similarly, the average Euclidean distance between \mathbf{x}_{i+t} and its neighbors is given by $L_{i+t} = \frac{1}{|N_\delta(\mathbf{x}_{i+t})|} \sum_{j=1}^{|N_\delta(\mathbf{x}_{i+t})|} \|\mathbf{x}_{i+t} - \mathbf{x}_{j+t}\|$. The scaling factor for the i -th observation is given by $\Delta S(t, i) = \frac{L_{i+t}}{L_i}$.

Fitting a linear regression to the average logarithm of scaling factors over all observations against each time step, we obtain an estimate of the maximum Lyapunov exponent λ of the underlying system from which the time series data was obtained.

We construct a similar pipeline to that of Kantz algorithm in order to estimate the persistence exponent of a real univariate time series via its state space embedding, which we call the *persistence exponent algorithm*. We provide a description of algorithm 2 for computing the persistence exponent. Given the i -th observation

Algorithm 1: Kantz algorithm to estimate the Lyapunov exponent

Inputs : $X, \delta, t_{\max}, t_{\text{initial}}, t_{\text{final}}$

- 1 Let N be the number of observations in the embedding X of a single time series.
- 2 for $\mathbf{x}_i \in X$,
- 3 find all $\mathbf{x}_j \in N_\delta(\mathbf{x}_i)$, excluding \mathbf{x}_i itself
- 4 compute L_i (Equation 3).
- 5 for $t \in 1, \dots, t_{\max}$,
- 6 identify all $\mathbf{x}_{j+t} \in N_\delta(\mathbf{x}_{i+t})$, excluding \mathbf{x}_{i+t} itself
- 7 compute L_{i+t}
- 8 store $\Delta S(t, i) = \frac{L_{i+t}}{L_i}$
- 9 $\lambda = \lim_{t \rightarrow t_{\max}} \log \left(\frac{1}{N} \sum_{i=1}^N \Delta S(t, i) \right)$ (fit a linear regression to $[t_{\text{initial}}, t_{\text{final}}]$)

Return: λ

\mathbf{x}_i in an embedding with N points, the 0-dimensional Betti vector from Vietoris-Rips filtration on its δ -neighborhood $N_\delta(\mathbf{x}_i) = \{\mathbf{x}_j : \|\mathbf{x}_i - \mathbf{x}_j\| < \delta\}$ is given by

$$\Delta \beta(\cdot, i) = \left(1, \dots, \frac{\beta_0^{\epsilon_r}(N_\delta(\mathbf{x}_i))}{\beta_0^{\epsilon_1}(N_\delta(\mathbf{x}_i))}, \dots, \frac{\beta_0^{\epsilon_R}(N_\delta(\mathbf{x}_i))}{\beta_0^{\epsilon_1}(N_\delta(\mathbf{x}_i))} \right),$$

where $\Delta \beta(r, i) = \frac{\beta_0^{\epsilon_r}(N_\delta(\mathbf{x}_i))}{\beta_0^{\epsilon_1}(N_\delta(\mathbf{x}_i))}$ corresponds to the the number of connected components in the Vietoris-Rips complex of the δ neighborhood of \mathbf{x}_i at the r -th filtration radius. Fitting a linear regression to the negative logarithm of the average Betti number among all observations against each filtration radius, we obtain an estimate of the persistence exponent β_{exp} of the underlying system from which the time series data was obtained.

Algorithm 2: Persistence exponent algorithm to estimate the persistence exponent

Inputs : $X, \delta, \text{epslist} = \{0 < \dots < \epsilon_r < \dots < \epsilon_R\}, \epsilon_{\text{initial}}, \epsilon_{\text{final}}$

- 1 Let N be the number of observations in the embedding X of a single time series.
- 2 for $\mathbf{x}_i \in X$,
- 3 find all $\mathbf{x}_j \in N_\delta(\mathbf{x}_i)$, *including* \mathbf{x}_i
- 4 initialize count = 0
- 5 for each $\epsilon_r \in \text{epslist}$,
- 6 for each $[b, d) \in \text{Bcd}_0(\mathcal{R}(N_\delta(\mathbf{x}_i)))$,
- 7 if $\epsilon_r \geq b$ and $\epsilon_r < d$,
- 8 count = count + 1
- 9 let $\beta_0^{\epsilon_r}(N_\delta(\mathbf{x}_i)) = \text{count}$
- 10 store $\Delta \beta(r, i) = \frac{\beta_0^{\epsilon_r}(N_\delta(\mathbf{x}_i))}{\beta_0^{\epsilon_1}(N_\delta(\mathbf{x}_i))}$ as the r th term in the Betti vector $\Delta \beta(\cdot, i)$
- 11 $\beta_{\text{exp}} = \lim_{r \rightarrow R} -\log \left(\frac{1}{N} \sum_{i=1}^N \Delta \beta(r, i) \right)$ (fit a linear regression to $[\epsilon_{\text{initial}}, \epsilon_{\text{final}}]$)

Return: β_{exp}

Remark 7.1 (Complexity of the persistence exponent algorithm). *In the worst case (for large δ), each observation \mathbf{x}_i in the embedding of a time series with N points has $N - 1$ neighbors so that $|N_\delta(\mathbf{x}_i)| = N - 1$. Hence computing the 0-dimensional persistent homology of $N_\delta(\mathbf{x}_i)$ requires $O(N \log N)$ computations [2]. We repeat this computation at most N times, once for every observation \mathbf{x}_i in the embedding. Hence algorithm 2 takes $O(N^2 \log N)$ time.*

8 Results

We compare the stability of our persistence exponent and the Lyapunov exponent when measuring chaos in two models of dynamical systems with known behavior—the Lorenz and Rossler systems. These systems model fluid convection and taffy pulling, respectively. We also compare the stability of both measures computed using algorithm 1 and algorithm 2 on real time series data of the Belousov-Zhabotinsky autocatalytic chemical reaction reported by Wodlei, Hristea, and Alberti [21]. We summarize our results in the corresponding subsections.

8.1 Lorenz System

The Lorenz system models fluid dynamics over time. The differentials $d\dot{X}/dt$, $d\dot{Y}/dt$, and $d\dot{Z}/dt$ indicate change in fluid convection, horizontal temperature variation, and vertical temperature variation of a fluid. Integrating these differentials and choosing three control parameter values $\mathbf{A} = \{\sigma, \beta, \rho\}$, we define the state space of this system as $(\dot{X}(\mathbf{A}, t), \dot{Y}(\mathbf{A}, t), \dot{Z}(\mathbf{A}, t)) \subset \mathbb{R}^3$. The parameters of \mathbf{A} describe the physical properties of the fluid, temperature difference in the fluid, and the physical properties of the overall system, respectively. This system is mathematically modeled as follows:

$$\begin{aligned}\dot{X} &= \sigma(y(t) - x(t)), \\ \dot{Y} &= x(t)(\rho - z(t)) - y(t), \\ \dot{Z} &= x(t)y(t) - \beta z(t).\end{aligned}$$

The default parameters are $\sigma = 10$ and $\beta = 8/3$, while ρ is varied to analyze system dynamics. Then the state space is given by $(\dot{X}(\rho, t), \dot{Y}(\rho, t), \dot{Z}(\rho, t))$, where a single trajectory within it is denoted as $\mathbf{x}_\rho(\mathcal{T}) = \{\mathbf{x}_\rho(t_0), \dots, \mathbf{x}_\rho(t_{T-1})\}$. A commonly selected initial condition is $\mathbf{x}_\rho(t_0) = (\dot{X}(\rho, t_0), \dot{Y}(\rho, t_0), \dot{Z}(\rho, t_0)) = (-13, -14, 47)$ [4]. We fix $\mathcal{T} = \{0, 0.01, \dots, 20\}$. We compute the average of each measure over 30 pairs of neighboring trajectories. For each pair of trajectories $\{\mathbf{x}_\rho(\mathcal{T}), \mathbf{y}_\rho(\mathcal{T})\}$, we define the initial conditions as $\mathbf{x}_\rho(t_0) = (-13, -14, 47) + \mathcal{N}(0, 0.1)$ and $\mathbf{y}_\rho(t_0) = \mathbf{x}_\rho(t_0) + \mathcal{N}(0, 0.0001)$, and the resulting trajectories by $\mathbf{x}_\rho^{d,\sigma}(\mathcal{T}) = \mathbf{x}_\rho^d(\mathcal{T}) + \mathcal{N}(0, \sigma \cdot \gamma_d)$ and $\mathbf{y}_\rho^{d,\sigma}(\mathcal{T}) = \mathbf{y}_\rho^d(\mathcal{T}) + \mathcal{N}(0, \sigma \cdot \omega_d)$, where γ_d and ω_d are the standard deviations of the d -th dimension of $\mathbf{x}_\rho(\mathcal{T})$ and $\mathbf{y}_\rho(\mathcal{T})$, respectively, for $d = 1, 2, 3$. We set $\rho = \{90, 90.1, \dots, 103\}$, $\sigma = \{0, 0.015, 0.025\}$, $\text{epslist} = \{0, 0.1, \dots, 8\}$, and fit β_{exp} and λ to $\epsilon = [0, 6]$ and $t = [0, 7]$, respectively.

See our results in Figure 3. As expected, our persistence exponent is much more robust to small trajectory perturbations when compared to the Lyapunov exponent. As well, our measure is also able to detect the periodicity around $\rho = 100.1$. Note that by Theorem 6.4 and our ϵ -fit, $0 \leq \beta_{\text{exp}}(X) \leq \frac{-\log\left(\frac{1}{2 \cdot (2000)}\right)}{6} \approx 1.38$.

8.2 Rossler System

The Rossler system models the ribbon-like folding of taffy that occurs when a taffy pulling machine runs [13]. This system experiences a period-doubling route to chaos, in which its periodicity gradually increases as its control parameter varies until it mimics chaotic behavior [5]. The differentials $d\dot{X}/dt$, $d\dot{Y}/dt$, and $d\dot{Z}/dt$ indicate changes in horizontal and vertical oscillatory behavior, and nonlinearity in the system over time. Integrating these differentials and choosing three control parameter values $\mathbf{A} = \{a, b, c\}$ defines the state space $(\dot{X}, \dot{Y}, \dot{Z}) \subset \mathbb{R}^3$. The parameters in \mathbf{A} control the linear stability, baseline drift, and chaoticity

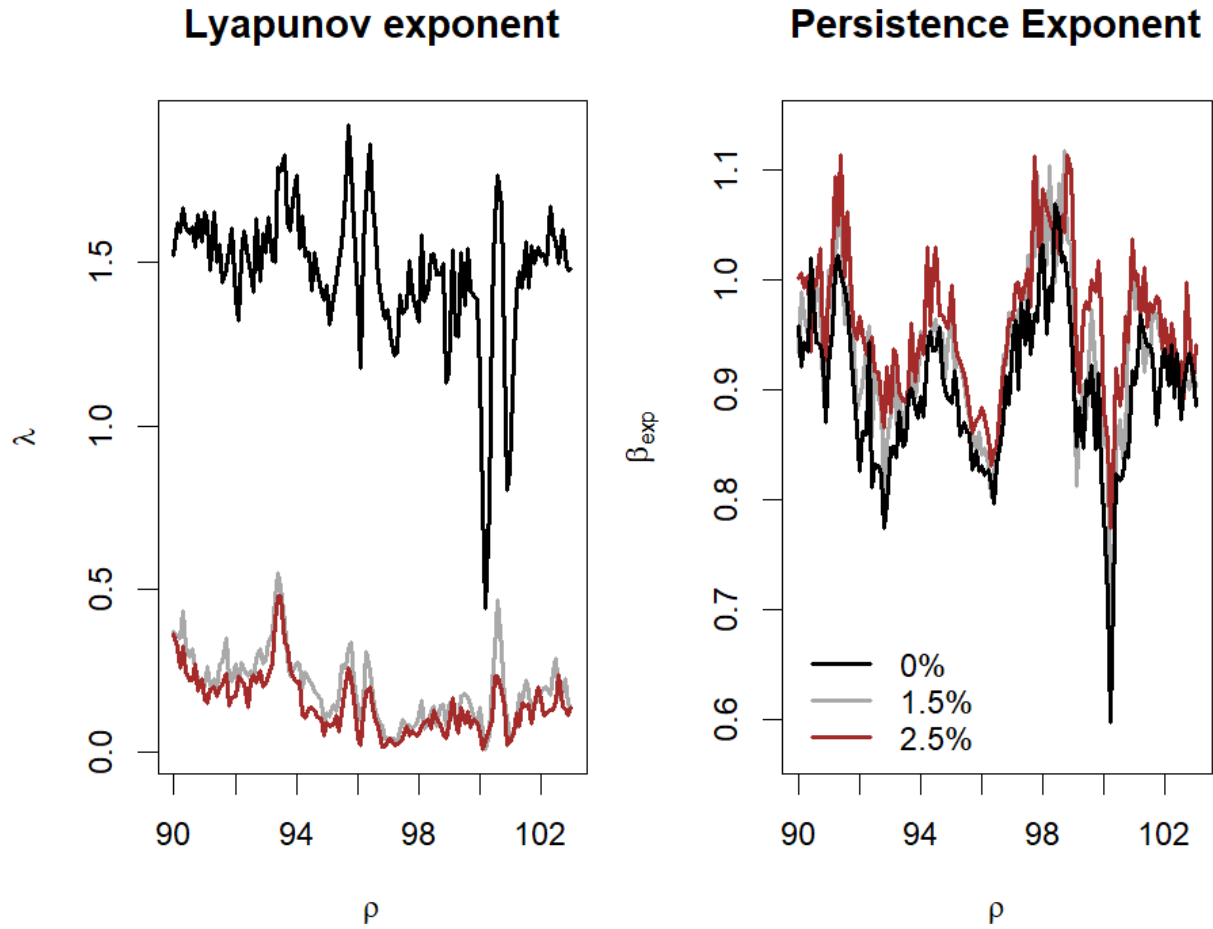


Figure 3: The average Lyapunov (left) and Persistence (right) exponents against increasing values of ρ for varied noise levels and initial conditions in the Lorenz system.

of the system, respectively. The Rossler system is modeled as follows.

$$\begin{aligned}\dot{X}(\mathbf{A}, t) &= -y(t) - z(t), \\ \dot{Y}(\mathbf{A}, t) &= x(t) + a \cdot y(t), \\ \dot{Z}(\mathbf{A}, t) &= b + z(t) \cdot (x(t) - c).\end{aligned}$$

For this experiment, we follow similar parametric choices as those used by Güzel, Munch, and Khasawneh [4]. That is, we fix $b = 2$ and $c = 4$, and vary a between 200 evenly-spaced values on $[0.37, 0.42]$. Then the state space is given by $(\dot{X}(a, t), \dot{Y}(a, t), \dot{Z}(a, t))$, where one of its trajectories is denoted as $\mathbf{x}_a(\mathcal{T}) = \{\mathbf{x}_a(t_0), \dots, \mathbf{x}_a(t_{T-1})\}$. We fix $\mathcal{T} = \{0, 1/15, \dots, 1000\}$. We compute the average exponents over 30 pairs of trajectories. For each pair of trajectories $\{\mathbf{x}_a(\mathcal{T}), \mathbf{y}_a(\mathcal{T})\}$, we define the initial conditions as $\mathbf{x}_a(t_0) = (-0.4, 0.6, 1) + \mathcal{N}(0, 0.001)$ and $\mathbf{y}_a(t_0) = \mathbf{x}_a(t_0) + \mathcal{N}(0, 0.0001)$, and the resulting trajectories by $\mathbf{x}_a^{d,\sigma}(\mathcal{T}) = \mathbf{x}_a^d(\mathcal{T}) + \mathcal{N}(0, \sigma \cdot \gamma_d)$ and $\mathbf{y}_a^{d,\sigma}(\mathcal{T}) = \mathbf{y}_a^d(\mathcal{T}) + \mathcal{N}(0, \sigma \cdot \omega_d)$, where γ_d and ω_d are the standard deviations of the d -th dimension of $\mathbf{x}_a(\mathcal{T})$ and $\mathbf{y}_a(\mathcal{T})$, respectively, for $d = 1, 2, 3$. We set $\sigma = \{0, 0.0015, 0.0025\}$,

$\text{epslist} = \{0, 0.001, \dots, 0.5\}$, and fit β_{exp} and λ to $\epsilon = [0, 0.15]$ and $t = [0, 100]$, respectively.

See our results in Figure 4. We can see that β_{exp} is much more stable given added noise for increasing a in comparison to λ . Both measures detect periodicity in a similar manner around $a \approx 0.4$ and $a \approx 0.41$.

Note that by Theorem 6.4 and our ϵ -fit, $0 \leq \beta_{\text{exp}}(X) \leq \frac{-\log\left(\frac{1}{2 \cdot (15000)}\right)}{0.2} \approx 68.72$.

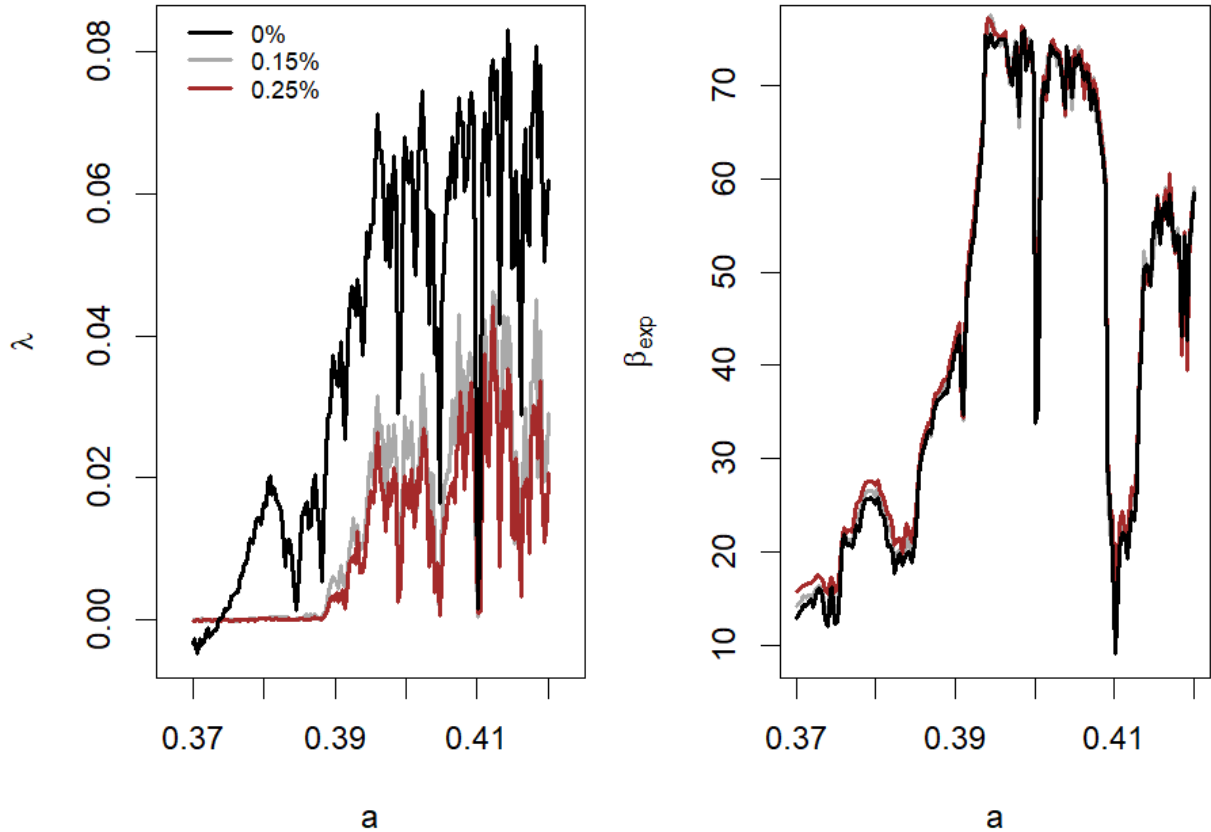


Figure 4: The average Lyapunov (left) and persistence (right) exponents against increasing values of a for varied noise levels and initial conditions in the Rossler system.

8.3 Real Time Series Data

In this section, we compare the average stability of the persistence and Lyapunov exponents of an auto-catalytic chemical reaction studied by Wodlei, Hristea, and Alberti [21]. We obtained a sped-up video of their experiment showing an unstirred, ferroin-catalyzed Belousov-Zhabotinsky reaction which captured the change in concentrations of the catalyst as the reaction progressed via a camera chip containing a color filter array. We followed their experimental instructions by using ImageJ to preprocess this video data into a single time series describing the average concentration of ferroin over time. We first extracted the average grayscale

(i.e., ferroin concentration) value of each column of pixels in the video over time via a multikymograph. To compute this graph, we extracted the average grayscale value of each column of 42 pixels centered at a yellow horizontal cross section in the video footage. We highlight one such column of pixels at a chosen time via a white rectangle in the left image of Figure 5. The corresponding average grayscale values over time for this column of pixels are summarized via the white horizontal cross section in multikymograph shown in the bottom right of Figure 5. The profile plot (i.e., time series) was then computed by averaging the grayscale values in each column of the multikymograph. We then denoised this series via a local projection filter [9]. Since we wanted to denoise while preserving as many points as possible and any chaotic structure present, and since chaos occurs in at least three dimensions, we performed the filter with an embedding dimension of three. We denote the resulting time series as $f_{\text{avg}}(\mathcal{T})$, for $\mathcal{T} = \{0, 1, \dots, 1527\}$ the horizontal pixel values. We define the corresponding embedding by $X = \text{SW}_{M, \tau} f_{\text{avg}}(\mathcal{T}) = (f_{\text{avg}}(\mathcal{T}), \dots, f_{\text{avg}}(\mathcal{T} + M\tau))$, where $\tau = 6$ and $M = 3$ are selected using the first minimum of the automutual information and Cao's False Nearest Neighbors test [20]. Hence our embedding satisfies $|X| = 1510$. We show a plot of $f_{\text{avg}}(\mathcal{T})$ and X in the top middle and top right images of Figure 5.

To compute the Lyapunov and persistence exponents using algorithm 1 and algorithm 2, we first fix $\delta = c \cdot D_X$, where D_X is the maximum pairwise distance between any two points in X . We choose $c = 0.07$ by varying $c \in [0.01, 0.20]$ and obtaining stable measures of $\lambda \in [0.006, 0.007]$ and $\beta_{\text{exp}} \in [0.434, 0.443]$ in the range $c \in [0.06, 0.08]$, choosing c as the mean value within this stable range. Hence, we define $\delta \approx 23.27$ and select 100 evenly spaced filtration radii ϵ_r in $[0, \delta]$. We fit our regression window for λ to $t = [0, 75]$ (i.e., $t_{\text{max}} = 75$, $t_{\text{initial}} = 0$, and $t_{\text{final}} = 75$), and for β_{exp} to $\epsilon = [0.2 \cdot \delta, 0.55 \cdot \delta]$ (i.e., $\epsilon_{\text{initial}} \approx 4.7$ and $\epsilon_{\text{final}} \approx 13.4$).

By Theorem 6.4, $0 \leq \beta_{\text{exp}}(X) \leq \frac{-\log\left(\frac{1}{|X|}\right)}{8.7} \approx 0.842$. We show the linear regressions and both exponents computed via algorithm 1 and algorithm 2 in the top left and right images of Figure 6, respectively. We can see that within this ϵ -range, our embedded time-series trajectory undergoes just over half of its total possible exponential divergence.

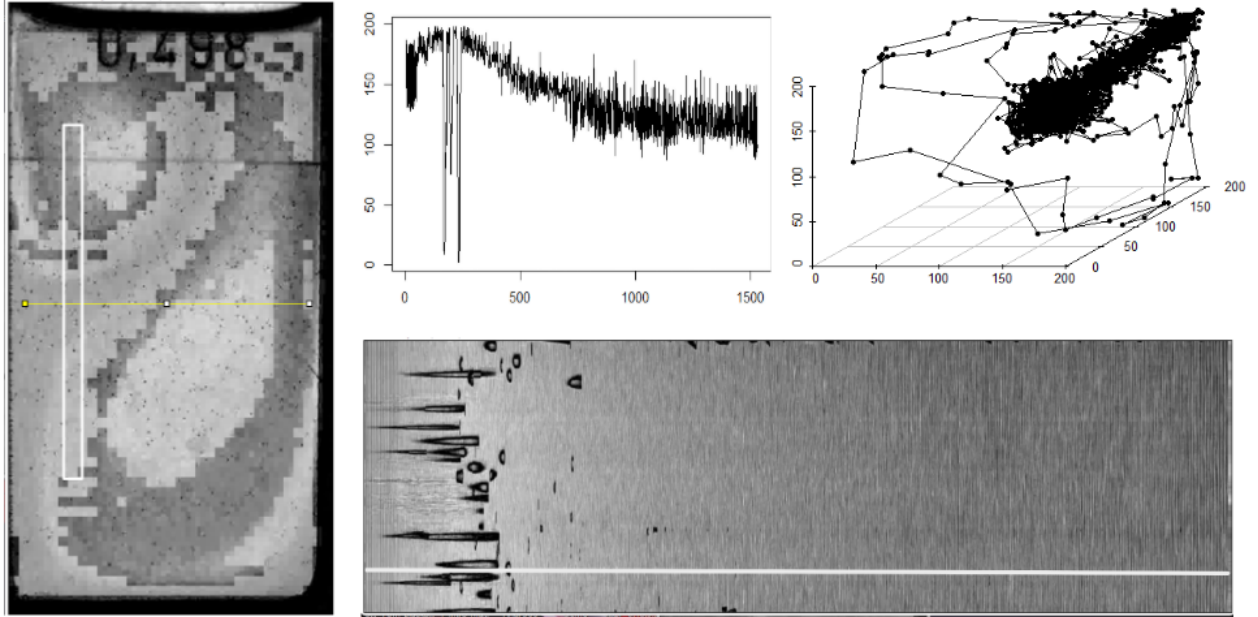


Figure 5: An Image-J screenshot of the video-d Belousov-Zhabotinski reaction [21] (left) and its resulting Kymograph (bottom right). We also show the resulting denoised profile plot of average ferroin concentrations (top middle) and its sliding windows embedding (top right).

For our stability analysis, we vary σ in $\{0.05, 0.1, \dots, 0.75\}$ and define the embedding of f_{avg} at noise

level σ as $X_\sigma = \text{SW}_{M,\tau} f_{\text{avg}}^\sigma(\mathcal{T})$, where $f_{\text{avg}}^\sigma(\mathcal{T}) = f_{\text{avg}}(\mathcal{T}) + \mathcal{N}(0, \sigma \cdot \gamma)$ is the time series at noise level σ and γ is the standard deviation of $f_{\text{avg}}(\mathcal{T})$. We finally compute the normalized average Lyapunov and persistence exponents of the single trajectory X_σ against σ over 30 samples of X_σ . For each σ , we fit our regressions for β_{exp} to $\epsilon \in [7, 13]$ and λ to $t \in [40, 80]$. We select our windows for t and ϵ by producing a random sample of λ and β_{exp} for each σ in the list $\{0.1, 0.2, \dots, 0.7\}$ and recording the window of best fit for each. We record windows for t and ϵ in the respective lists $\{[7, 13], [7, 15], [7, 17], [7, 20]\}$ and $\{[40, 80], [30, 80], [20, 80], [20, 90]\}$, choosing their intersections as the regression windows for each measure. In Figure 6, we can see that when adding up to 20% Gaussian noise to $f_{\text{avg}}(\mathcal{T})$ (i.e., $\sigma \leq 0.2$), our Persistence exponent is more stable in comparison, as indicated by the normalized measures within the red vertical dashed lines laying between $[0.886, 1]$ for λ and $[0.976, 1]$ for β_{exp} .

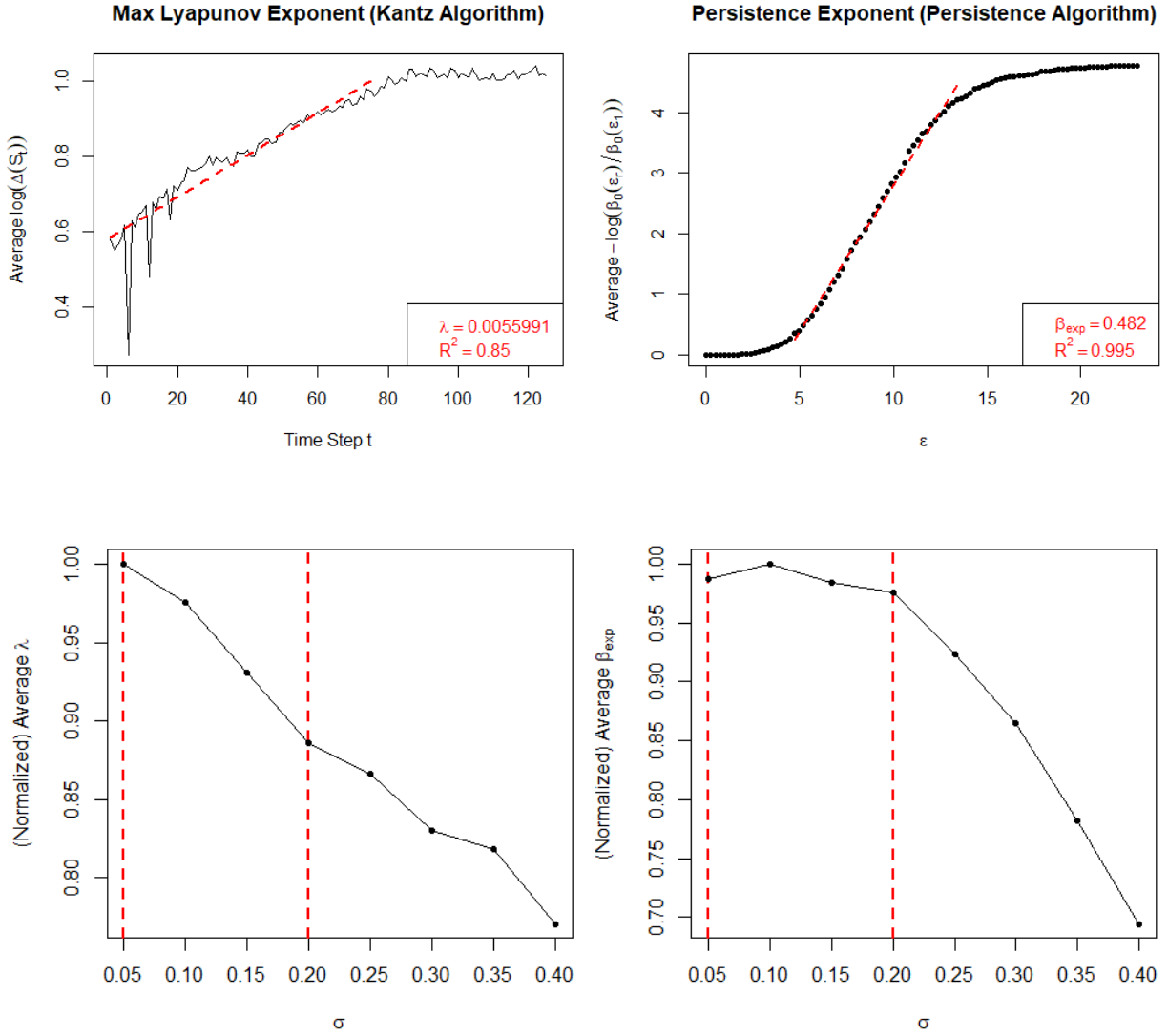


Figure 6: The Lyapunov (top left) and persistence (top right) exponents of the Belousov-Zhabotinsky reaction [21]. We also plot the normalized averages of the Lyapunov (bottom left) and persistence (bottom right) exponents against increasing Gaussian noise levels added to the time series of this reaction.

9 Discussion

Although our work successfully provides a stable alternative to the Lyapunov exponent for noisy data, we are interested in exploring extensions of our exponent to higher homology dimensions. However, in any dimension greater than zero, stability of the Betti number is not guaranteed, so we may want to explore the use of a stable Betti number [15] to construct such a chaos measure. Persistent homology has also been used to construct a measure of quasiperiodicity for systems [19]. We have shown our measure to be robust to added noise in systems displaying period-doubling routes to chaos (i.e., the Rossler system). However, we are interested in using this quasiperiodicity measure to construct a measure of chaos robust to added noise for systems that undergo a quasiperiodic route to chaos [5]. We further want to explore algorithm optimization for algorithm 2 as well as analyzing the behavior of β_{exp} for varying control parameters in higher dimensions (i.e., when we vary more than one parameter at a time to detect dynamic behavior). Furthermore, for systems whose dynamics are better described by more than one parameter, we are interested in constructing a measure for chaos via multiparameter persistent homology.

References

- [1] Frédéric Chazal, Vin de Silva, and Steve Oudot. Persistence stability for geometric complexes. *Geometriae Dedicata*, 173:193–214, 2014. doi:10.1007/s10711-013-9937-z.
- [2] Marc Glisse. Fast persistent homology computation for functions on \mathbb{R} , 2023. URL: <https://arxiv.org/abs/2301.04745>, arXiv:2301.04745.
- [3] Peter Grassberger and Itamar Procaccia. Measuring the strangeness of strange attractors. *Physica D: Nonlinear Phenomena*, 9(1):189–208, 1983. doi:10.1016/0167-2789(83)90298-1.
- [4] İsmail Güzel, Elizabeth Munch, and Firas A. Khasawneh. Detecting bifurcations in dynamical systems with CROCKER plots. *Chaos: An Interdisciplinary Journal of Nonlinear Science*, 32(9):093111, 09 2022. doi:10.1063/5.0102421.
- [5] Robert C. Hilborn. *Chaos and Nonlinear Dynamics, An Introduction for Scientists and Engineers*. Oxford University Press, New York, 2nd edition, 2006.
- [6] W. Hussain Shah, S. Rafia Fatima, G. Huerta-Cuellar, J. H. García-López, C. G. Mata Ramirez, and R. Jaimes-Reátegui. Topological data analysis approach to time series and shape analysis of dynamical system. *Chaos: An Interdisciplinary Journal of Nonlinear Science*, 35(6):063129, 06 2025. doi:10.1063/5.0268340.
- [7] Jonathan Jaquette and Benjamin Schweinhart. Fractal dimension estimation with persistent homology: A comparative study. *Communications in Nonlinear Science and Numerical Simulation*, 84:105163, 2020. doi:10.1016/j.cnsns.2019.105163.
- [8] Holger Kantz. A robust method to estimate the maximal Lyapunov exponent of a time series. *Physics Letters A*, 185(1):77–87, 1994. doi:10.1016/0375-9601(94)90991-1.
- [9] Holger Kantz and Thomas Schreiber. *Nonlinear Time Series Analysis*. Cambridge University Press, 2 edition, 2003.
- [10] Michael Lesnick. The Theory of the Interleaving Distance on Multidimensional Persistence Modules. *Foundations of Computational Mathematics*, 15(3):613–650, jun 2015. doi:10.1007/s10208-015-9255-y.
- [11] Khushboo Mittal and Shalabh Gupta. Topological characterization and early detection of bifurcations and chaos in complex systems using persistent homology. *Chaos: An Interdisciplinary Journal of Nonlinear Science*, 27(5):051102, 05 2017. doi:10.1063/1.4983840.

- [12] Jose Perea and John Harer. Sliding Windows and Persistence: An Application of Topological Methods to Signal Analysis. *Foundations of Computational Mathematics*, 15:799–838, 2015. [arXiv:1307.6188](https://arxiv.org/abs/1307.6188), doi:10.1007/s10208-014-9206-z.
- [13] Otto E. Rössler. The chaotic hierarchy. *Zeitschrift für Naturforschung A*, 38(7):788–801, 1983. doi:10.1515/zna-1983-0714.
- [14] M. Rüdisüli, T.J. Schildhauer, S.M.A. Biollaz, and J.R. Van Ommen. 18 - Measurement, monitoring and control of fluidized bed combustion and gasification. In Fabrizio Scala, editor, *Fluidized Bed Technologies for Near-Zero Emission Combustion and Gasification*, Woodhead Publishing Series in Energy, pages 813–864. Woodhead Publishing, 2013. doi:10.1533/9780857098801.3.813.
- [15] Martina Scolamiero, Wojciech Chacholski, Anders Lundman, Ryan Ramanujam, and Sebastian Öberg. Multidimensional Persistence and Noise. *Foundations of Computational Mathematics*, 17(6):1367–1406, dec 2017. doi:10.1007/s10208-016-9323-y.
- [16] W. Hussain Shah, R. Jaimes-Reátegui, G. Huerta-Cuellar, J.H. García-López, and A.N. Pisarchik. Persistent homology approach for uncovering transitions to chaos. *Chaos, Solitons & Fractals*, 192:116054, 2025. doi:10.1016/j.chaos.2025.116054.
- [17] Vladimir Sharafutdinov and Clayton Shonkwiler. The Complete Dirichlet-to-Neumann Map for Differential Forms. *Journal of Geometric Analysis*, 23(4):2063–2080, 10 2013. doi:10.1007/s12220-012-9320-6.
- [18] Joshua R. Tempelman and Firas A. Khasawneh. A look into chaos detection through topological data analysis. *Physica D: Nonlinear Phenomena*, 406:132446, 2020. doi:10.1016/j.physd.2020.132446.
- [19] Christopher J. Tralie and Jose A. Perea. (Quasi)Periodicity Quantification in Video Data, Using Topology. *SIAM Journal on Imaging Sciences*, 11(2):1049–1077, 2018. doi:10.1137/17M1150736.
- [20] Sebastian Wallot and Giuseppe Leonardi. Analyzing Multivariate Dynamics Using Cross-Recurrence Quantification Analysis (CRQA), Diagonal-Cross-Recurrence Profiles (DCRP), and Multidimensional Recurrence Quantification Analysis (MdRQA) – A Tutorial in R. *Frontiers in Psychology*, 9, 2018. doi:10.3389/fpsyg.2018.02232.
- [21] Florian Wodlei, Mihnea R. Hristea, and Giuseppe Alberti. Periodic Motion in the Chaotic Phase of an Unstirred Ferroin-Catalyzed Belousov Zhabotinsky Reaction: Dataset. *Frontiers in Chemistry*, 10, 2022. doi:10.3389/fchem.2022.881691.